Supporting Information

Borate intercalation optimizes the electro-oxidation kinetics of α-$Ni(OH)_2$ nanosheets for selective electrochemical conversion of benzylamine to benzonitrile

*Zhongcheng Wang, Fengjuan Guo, Xusheng Zhang, Hongtao Gao and Wenlong Yang**

Z. C. Wang, F. J. Guo, X. S. Zhang, Prof. H. T. Gao, Prof. W. L. Yang
Key Laboratory of Optic-electric Sensing and Analytical Chemistry for Life Science, MOE, Key Laboratory of Analytical Chemistry for Life Science in Universities of Shandong, College of Chemistry and Molecular Engineering, Qingdao University of Science and Technology, Qingdao 266042, P. R. China
E-mail: wlyang@qust.edu.cn

Experimental Section

Product characterization: The oxidation products after the BA electrolysis at different potentials in the electrolyte were extracted with ethyl acetate and then qualitatively and quantitatively analyzed with gas chromatography-mass spectrometer (GCMS-QP2020) by applying bromobenzene as an internal standard. The drainage strategy was applied to measure the volume of the as-formed H_2 at cathode during the two-electrode electrolysis.

The FEs for the BN and H_2 production were calculated as follows:

$$FE_{BN}(\%) = \frac{mol\ of\ \ BN}{total\ passed\ charge/4F} \times 100\%$$

$$FE_{H2}(\%) = \frac{mol\ of\ \ hydrogen}{total\ passed\ charge/2F} \times 100\%$$

Where F is the Faraday constant (96485 C mol^{-1}).

Calculation Method: In this work, the first-principles DFT calculations were carried out using the projector-augmented wave (PAW) method[1] and the Perdew−Burke−Ernzerhof (PBE) exchange-correlation functional within the generalized gradient approximation (GGA) as implemented in the Vienna Ab-initio Simulation Package (VASP).[2,3] The van der Waals interactions were described by the dispersion correction of the DFT-D3 technique.[4] The plane-wave energy cutoff was set to 520 eV. All of the atoms were fully relaxed, and the convergence criterion for residual forces and energies was set at 0.02 eV/Å and 10^{-5} eV, respectively. The K-points for the Brillouin-zone integration were sampled by the Monkhorst-Pack scheme applying 3×3×1 and 9×9×1 grids for structure optimization and electronic properties calculations, respectively. A 20 Å z-direction vacuum space was employed to avert the mutual effects between periodic mirrors. DFT+U methods were applied to describe the localized 3d electron correlation for transition metal Ni, by considering on-site Coulomb (U) and exchange (J) interactions, and the Hubbard ‘U’ was set to 6 eV. Moreover, the Materials Studio and VASPKIT codes were used for modeling and processing VASP results, respectively.[5-7]

The C_7H_9N adsorption energy for P-$Ni(OH)_2$ and BI-$Ni(OH)_2$ was calculated by the following equation:

$$\Delta E = E_{total} - E_{surface} - E_{C7H9N} \quad (1)$$

where E_{total} represents the total energy of P-$Ni(OH)_2$ and BI-$Ni(OH)_2$ after adsorption C_7H_9N molecules, $E_{surface}$ is the energy of P-$Ni(OH)_2$ and BI-$Ni(OH)_2$, and E_{C7H9N} is the energy of adsorbate C_7H_9N molecule.

The Gibbs free energy potential of reaction intermediates for the BOR was calculated according to the computational hydrogen electrode (CHE) model proposed by Nørskov et al.[8] The change of Gibbs free energy for each elementary step can be calculated with the following equation:

$$\Delta G = \Delta E_{DFT} + \Delta E_{ZPE} - T\Delta S + \Delta G_U + \Delta G_{pH} \quad (2)$$

where ΔE_{DFT} is the electronic energy difference between the products and reactants gained from DFT calculations, ΔZPE and $T\Delta S$ are the correction of zero-point energy and the variation of vibrational entropy, respectively, which can be obtained *via* the vibrational frequency calculation at T=298.15 K. For gaseous molecules, entropies were obtained from the NIST Chemistry Website.[9] ΔG_U is the contribution of the external potential, and its values are equal to -n eU, in which n is the number of electrons transported and U is the applied voltage. ΔG_{pH} is the Gibbs free energy correction based on H^+ concentration, and it can be defined as follows:

$$\Delta G_{pH} = -k_B T \ln[H^+] = pH \times k_B T \ln 10 = 2.303 k_B T pH \quad (3)$$

where k_B is the Boltzmann constant, and in this work, pH was set to zero.

The charge density difference is calculated as in Equation (3) to display the charge redistribution, which reveals the electron transfer between the interface of $B_4O_9H_4$ and $Ni(OH)_2$.

$$\Delta\rho = \rho_{BI\text{-}Ni(OH)2} - \rho_{B4O9H4} - \rho_{Ni(OH)2} \quad (4)$$

where the $\rho_{BI\text{-}Ni(OH)2}$, ρ_{B4O9H4}, and $\rho_{Ni(OH)2}$ represent the electron density of BI-$Ni(OH)_2$ system, $B_4O_9H_4$, and $Ni(OH)_2$, respectively.

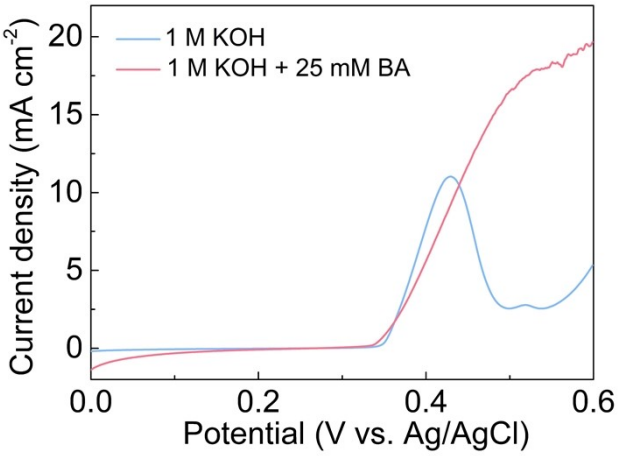

Figure S1. LSV curves of P-Ni(OH)$_2$ nanosheets in 1.0 M KOH with and without 25 mM BA at a scan rate of 5 mV s^{-1}.

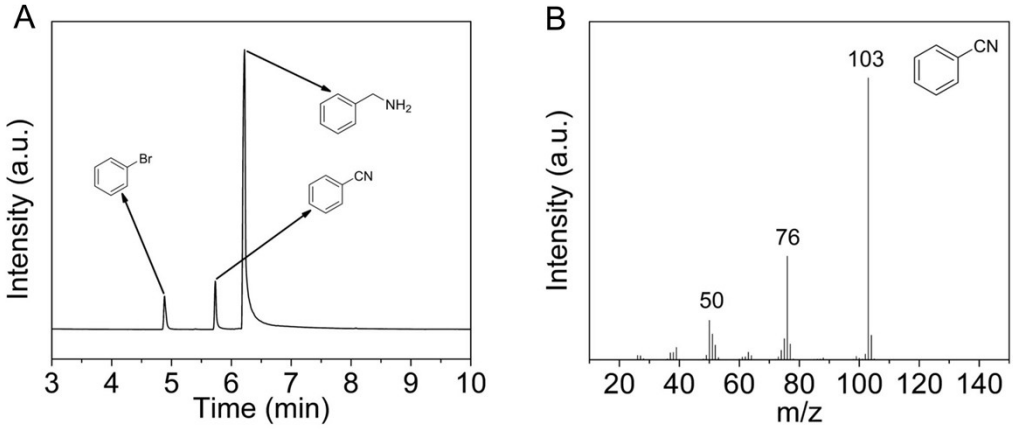

Figure S2. Product characterization after the BA electrolysis: (A) The gas chromatography and (B) mass spectrometer. Bromobenzene was employed as an internal standard.

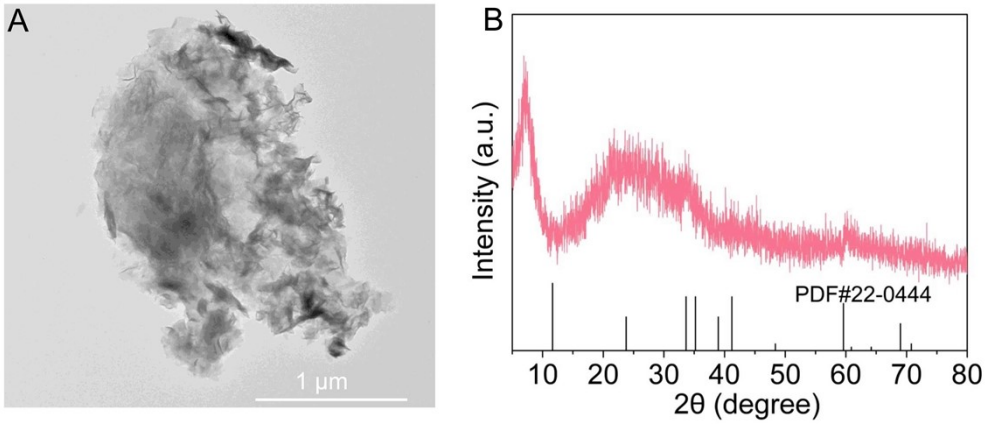

Figure S3. (A) TEM image and (B) XRD pattern of BI-Ni(OH)$_2$ nanosheets after stability test.

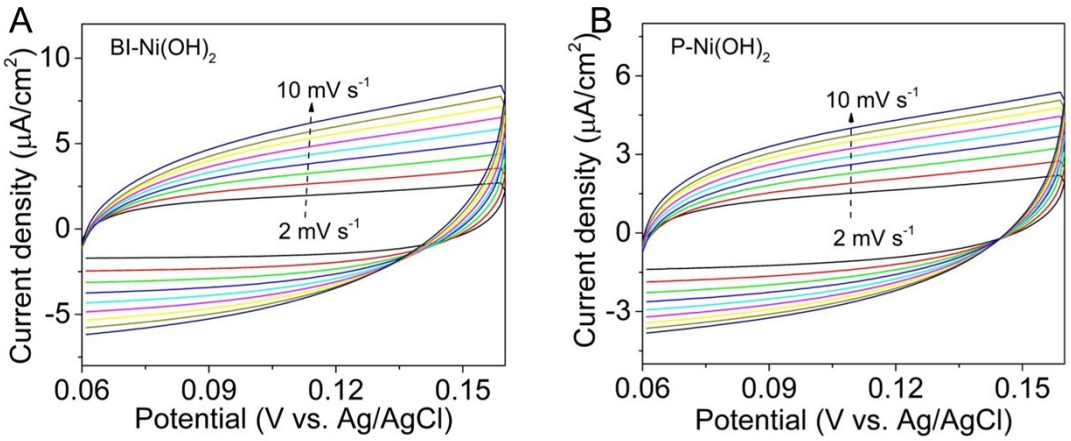

Figure S4. CV curves of (A) BI-Ni(OH)$_2$ and (B) P-Ni(OH)$_2$ measured in 1.0 M KOH at scan rates from 2 to 10 mV s^{-1}.

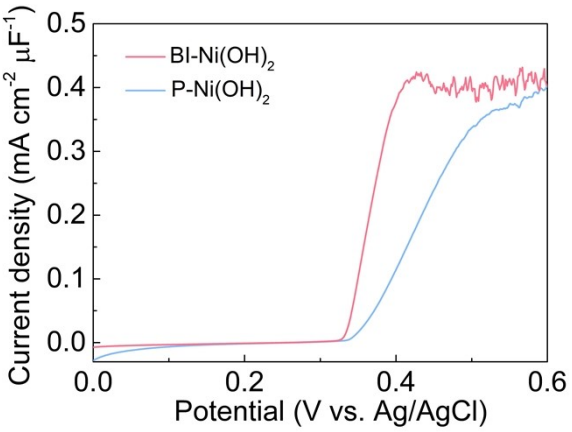

Figure S5. LSV curves normalized by the corresponding C_{dl} values of BI-Ni(OH)$_2$ and P-Ni(OH)$_2$ nanosheets.

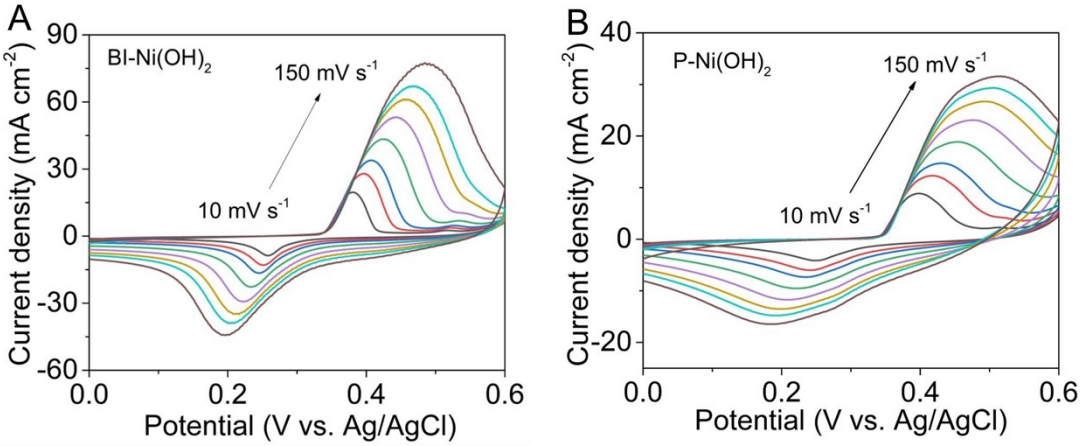

Figure S6. CV curves of (A) BI-Ni(OH)$_2$ and (B) P-Ni(OH)$_2$ in 1.0 M KOH at various scan rates of 10, 20, 50, 75, 100, 120 and 150 mV s^{-1}.

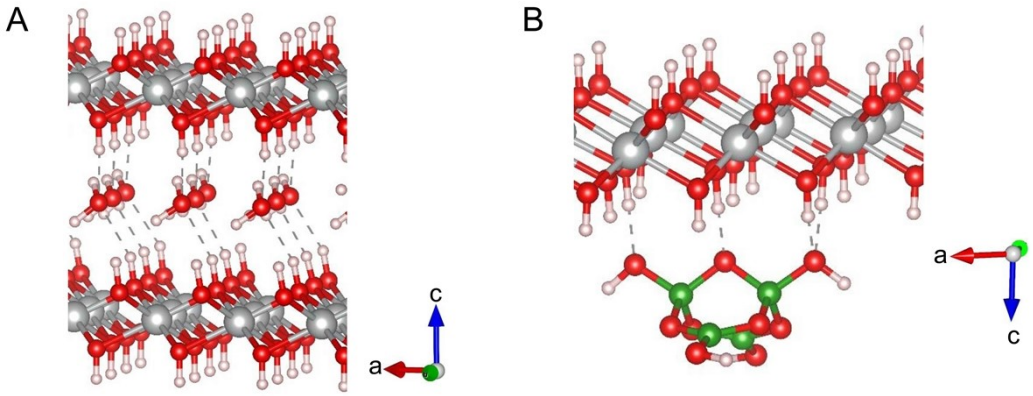

Figure S7. The optimized structure models of (A) P-$Ni(OH)_2$ and (B) BI-$Ni(OH)_2$.

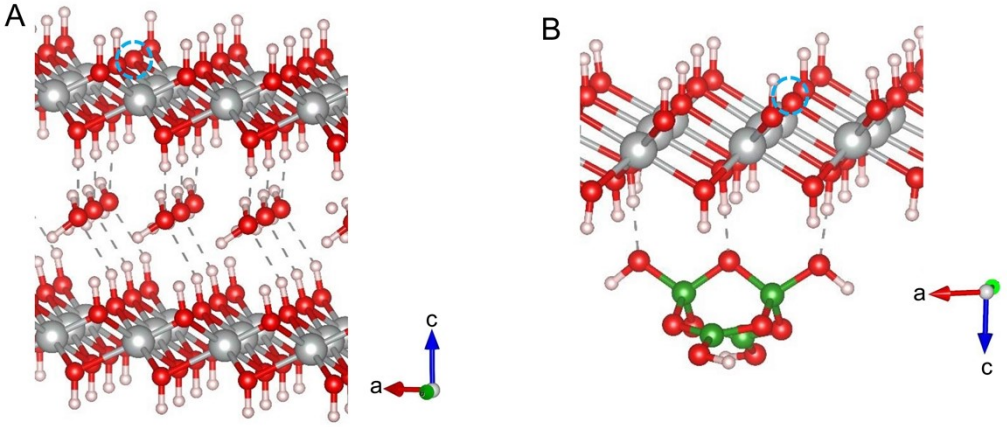

Figure S8. The corresponding structures of the dehydrogenation reaction from $Ni(OH)_2$ to NiOOH for (A) P-$Ni(OH)_2$ and (B) BI-$Ni(OH)_2$.

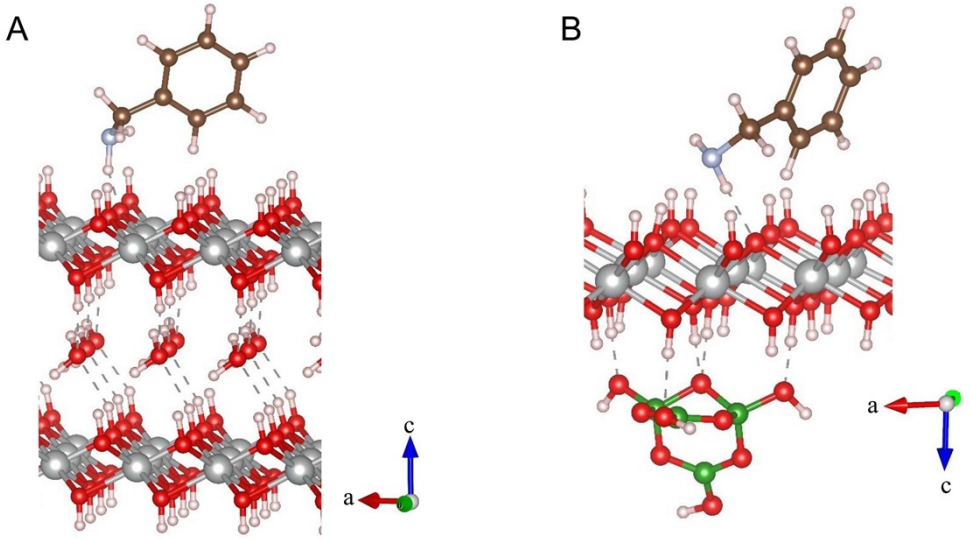

Figure S9. The BA adsorption on (A) P-$Ni(OH)_2$ and (B) BI-$Ni(OH)_2$.

Table S1. Comparison of the electrochemical BOR performance between the BI-$Ni(OH)_2$ electrode and other high-efficiency catalysts recently reported.

Catalyst	Onset potential (V vs. RHE)	FE (%)	Electrolyte
BI-$Ni(OH)_2$, this work	1.35	81.4	1 M KOH + 25 mM BA
Mn-α-$Ni(OH)_2$[10]	1.31	96	1 M KOH + 25 mM BA
Fe-doped Ni_3S_2[11]	~1.33	99	1 M KOH + 10 mM BA
NiSe[12]	1.34	99	1 M KOH + 25 mM BA
$Mo_{0.8}Ni_{0.2}N$-Ni_3N/NF[13]	~1.37	97	0.1 M KOH + 0.5 M Na_2SO_4 + 25 mM BA
Ni_3N[14]	~1.35	~95	1 M KOH + 2 mmol BA
CuCo-$Ni(OH)_2$[15]	~1.32	90.2	1 M KOH+10 mM BA
Ni_2Co-LDH/rGO[16]	~1.30	~85	1 M KOH+100 mM BA
W-doped Ni_2P[17]	~1.32	95	1 M KOH + 25 mM BA
NiCoFe-CAT[18]	1.29	~87	1 M KOH + 10 mM BA

Table S2. The calculated NiOOH formation energies and BA adsorption energies of on P-$Ni(OH)_2$ and BI-$Ni(OH)_2$ surfaces. Unit: eV.

Species	$\triangle E_H$ (eV)	$\triangle E_{C7H9N}$ (eV)
P-$Ni(OH)_2$	2.76	-0.83
BI-$Ni(OH)_2$	2.16	-1.17

Table S3. The calculated intermediate energies on the P-$Ni(OH)_2$ surface, unit: eV.

	E	ΔZPE-TΔS	G		ΔG
surface	-576.19	-	-576.19	*+C_7H_9N	0
C_7H_9N*	-681.579	3.643	-677.936	C_7H_9N*	-0.939
C_7H_8N*	-677.973	3.448	-674.525	C_7H_8N*	0.701544
C_7H_7N*	-673.269	3.136	-670.133	C_7H_7N*	1.682544
C_7H_6N*	-668.821	2.76	-666.061	C_7H_6N*	1.362544
C_7H_5N*	-665.305	2.49	-662.815	C_7H_5N*	0.536544
H_2O	-14.23	0.000544	14.229456	*+C_7H_5N	0.185
OH^-	-11.52		-11.52		
C_7H_9N	-104.556	3.749	-100.807		
C_7H_5N	-88.921	2.481	-86.44		

Table S4. The calculated intermediates energies on BI-Ni$(OH)_2$ surface, unit: eV.

	E	ΔZPE-TΔS	G		ΔG
surface	-335.772	-	-335.772	*+C_7H_9N	0
C_7H_9N*	-441.501	3.7	-437.801	C_7H_9N*	-1.222
C_7H_8N*	-437.448	3.478	-433.97	C_7H_8N*	1.121544
C_7H_7N*	-434.363	4.429	-429.934	C_7H_7N*	1.326544
C_7H_6N*	-429.667	2.838	-426.829	C_7H_6N*	0.395544
C_7H_5N*	-425.472	2.555	-422.917	C_7H_5N*	1.202544
H_2O	-14.23	0.000544	-14.22946	*+C_7H_5N	0.705
OH^-	-11.52	-	-11.52		
C_7H_9N	-104.556	3.749	-100.807		
C_7H_5N	-88.921	2.481	-86.44		

References

[1] G. Kresse, J. Furthmüller, *Phys. Rev. B*, **1996**, *54*, 11169.

[2] G. Kresse, D. Joubert, *Phys. Rev. B*, **1999**, *59*, 1758.

[3] J. P. Perdew, K. Burke, M. Ernzerhof, *Phys. Rev. Lett.*, **1996**, *77*, 3865.

[4] S. Grimme, J. Antony, S. Ehrlich, H. Krieg, *J. Chem. Phys.*, **2010**, *132*, 154104.

[5] J. Yu, Y. Zhao, X. Niu, J. Li, H. Gao, *Int. J. Hydrogen Energy*, **2022**, *47*, 29622.

[6] J. Jia, B. J. Li, S. Q. Duan, Z. Cui, H. T. Gao, *Nanoscale*, **2019**, *11*, 20307.

[7] V. Wang, N. Xu, J. C. Liu, G. Tang, W. T. Geng, *Comput. Phys. Commun.*, **2021**, *267*, 108033.

[8] J. K. Nørskov, J. Rossmeisl, A. Logadottir, L. Lindqvist, J. R. Kitchin, T. Bligaard, H. Jónsson, *J. Phys. Chem. B*, **2004**, *108*, 17886.

[9] P. J. Linstrom, W.G. Mallard, *J. Chem. Eng. Data*, **2001**, *46*, 1059.

[10] Y. X. Sun, H. Shin, F. Y. Wang, B. L. Tian, C. W. Chiang, S. T. Liu, X. S. Li, Y. Q. Wang, L. Y. Tang, W. A. Goddard, M. N. Ding, *J. Am. Chem. Soc.* **2022**, *144*, 15185.

[11] L. Z. Sun, Z. Y. Zhou, Y. N. Xie, J. G. Zheng, X. Pan, L. N. Li, G. H. Zhao, *Adv. Funct. Mater.* **2023**, *33*, 2301884.

[12] Y. Huang, X. D. Chong, C. B. Liu, Y. Liang, B. Zhang, *Angew. Chem. Int. Ed.* **2018**, *57*, 13163.

[13] Y. Li, Y. Q. Jiao, H. J. Yan, G. C. Yang, Y. Liu, C. G. Tian, A. P. Wu, H. G. Fu, *Angew. Chem. Int. Ed.* **2023**, *62*, e202306640.

[14] F. H. Ma, S. H. Wang, L. Y. Han, Y. H. Guo, Z. Y. Wang, P. Wang, Y. Y. Liu, H. F. Cheng, Y. Dai, Z. K. Zheng, B. B. Huang, *ACS Appl. Mater. Interfaces* **2021**, *13*, 56140.

[15] M. M. Song, M. M. Feng, F. Li, S. S. Lv, Y. Zhou, Z. Chen, *Inorg. Chem.* **2024**, *63*, 15215.

[16] R. C. Sahoo, S. Paniya, R. Singh, A. M. Pai, K. Vankayala, H. S. S. R. Matte, *ACS Appl. Nano Mater.* **2024**, *7*, 26457.

[17] Z. T. Tu, X. Y. He, X. Liu, D. K. Xiong, J. Zuo, D. L. Wu, J. Y. Wang, Z. F. Chen, *Chin. J. Catal.* **2024**, *58*, 146.

[18] Y. Wang, Y. Y. Xue, L. T. Yan, H. P. Li, Y. P. Li, E. H. Yuan, M. Li, S. N. Li, Q. G. Zhai, *ACS Appl. Mater. Interfaces* **2020**, *12*, 24786.